ELSEVIER

Remote Sensing of Environment 83 (2002) 414–430

Remote Sensing of Environment

www.elsevier.com/locate/rse

# Multiscale analysis and validation of the MODIS LAI product I. Uncertainty assessment

Yuhong Tian [a,b,*], Curtis E. Woodcock [a], Yujie Wang [a], Jeff L. Privette [c], Nikolay V. Shabanov [a], Liming Zhou [b], Yu Zhang [a], Wolfgang Buermann [a], Jiarui Dong [a], Brita Veikkanen [d], Tuomas Häme [d], Kaj Andersson [d], Mutlu Ozdogan [a], Yuri Knyazikhin [a], Ranga B. Myneni [a]

[a] *Department of Geography, Boston University, Boston, MA 02215, USA*
[b] *School of Earth and Atmospheric Sciences, Georgia Institute of Technology, Atlanta, GA 30332, USA*
[c] *Code 923, NASA Goddard Space Flight Center, Greenbelt, MD 20771, USA*
[d] *VTT AUTOMATION, Remote Sensing, 02044 VTT, Finland*

Received 16 November 2001; received in revised form 5 April 2002; accepted 7 April 2002

**Abstract**

The development of appropriate ground-based validation techniques is critical to assessing uncertainties associated with satellite data-based products. Here we present a method for validation of the Moderate Resolution Imaging Spectroradiometer (MODIS) Leaf Area Index (LAI) product with emphasis on the sampling strategy for field data collection. This paper, the first of two-part series, details the procedures used to assess uncertainty of the MODIS LAI product. LAI retrievals from 30 m ETM+ data were first compared to field measurements from the SAFARI 2000 wet season campaign. The ETM+ based LAI map was thus as a reference to specify uncertainties in the LAI fields produced from MODIS data (250-, 500-, and 1000-m resolutions) simulated from ETM+. Because of high variance of LAI measurements over short distances and difficulties of matching measurements and image data, a patch-by-patch comparison method, which is more realistically implemented on a routine basis for validation, is proposed. Consistency between LAI retrievals from 30 m ETM+ data and field measurements indicates satisfactory performance of the algorithm. Values of LAI estimated from a spatially heterogeneous scene depend strongly on the spatial resolution of the image scene. The results indicate that the MODIS algorithm will underestimate LAI values by about 5% over the Maun site if the scale of the algorithm is not matched to the resolution of the data.


## 1. Introduction

Leaf Area Index (LAI), the green leaf area per unit ground area, is a key biophysical variable influencing vegetation photosynthesis, transpiration, and the energy balance of the land surface (Bonan, 1995; Running, 1990). LAI is not only an important driver of most ecosystem productivity models operating at landscape to global scales (Running, Nemani, Peterson, et al., 1989; Turner, Cohen, Kennedy, Fassnacht, & Briggs, 1999), but also an interaction component of some general circulation models (Buermann, Dong, Zeng, Myneni, & Dickinson, 2001). LAI, together with other biophysical variables, plays an important role in measurement and monitoring of land surface characteristics and in the development of earth-system models that potentially can predict large-scale changes accurately enough to assist policy makers in making decisions concerning the management of our environment (Cohen & Justice, 1999). In view of this need, LAI is a standard product to be delivered from data acquired by the Moderate Resolution Imaging Spectroradiometer (MODIS) aboard the Earth Observing System (EOS) Terra platform. As MODIS LAI data products begin to be available to the public through the EROS data centre Data Active Archive Center (EDC DAAC), a sustained validation program is needed to provide timely feedback to algorithm developers so that through iterative improvements, product quality can be improved (Privette et al., 2000).

"Validation" is the process of assessing by independent means the accuracy of data products (Justice et al., 2000; Privette et al., 2000). In general, validation refers to assessing the uncertainty of satellite-derived products by analytical comparison to reference data (e.g., *in situ*, air-

* Corresponding author. School of Earth and Atmospheric Sciences, Georgia Institute of Technology, 221 Bobby Dodd Way, Atlanta, GA 30332, USA. Tel.: +1-404-385-2383; fax: +1-404-385-1510.
*E-mail address:* ytian@eas.gatech.edu (Y. Tian).

0034-4257/02/$ - see front matter © 2002 Elsevier Science Inc. All rights reserved.
PII: S0034-4257(02)00047-0

craft, and high-resolution satellite sensor data), which are presumed to represent the target values (Justice et al., 2000).

Validation of satellite products comes at a time when international agencies and the global change research community are evaluating their needs for long-term spaceborne measurements (Justice et al., 2000). In the coming years, several moderate and coarse spatial resolution satellite sensors such as AVHRR, GLI, MERIS, MISR, MODIS, POLDER, VEGETATION, etc. will concurrently fly, providing multiple views daily of the Earth surface. These sensors will provide similar land products, such as vegetation indices, LAI, FPAR, albedo, and land cover (Justice et al., 2000; Weiss et al., 2001). Establishing standard methods and protocols for validation of these products will enable broad participation in validation campaigns. As a result, high-quality and consistent data sets of known accuracy with product continuity between instruments and missions will foster product standardization and synergy from these sensors (Justice et al., 2000).

NASA has developed validation protocols and organized several pre- and post-launch validation campaigns. The "BigFoot" program is one such protocol designed for the validation of MODIS land cover, LAI, FPAR, and NPP products, providing guidance for field data collection, sampling strategy, and scaling algorithms to compare to the ground, airborne and satellite sensor data (Cohen & Justice, 1999). The Prototype Validation Exercises (PROVE) were designed and carried out as a prototype of EOS episodic validation campaigns (Privette et al., 2000). The Southern Africa Regional Initiative 2000 (SAFARI 2000) took place during 1999 and 2000 in Southern African as an extensive validation effort associated with EOS Terra and Landsat 7. Internationally, the VALidation of European Remote sensing Instruments (VALERI) project is designed to provide coordinated ground measurements of LAI, FPAR, albedo and similar variables for developing and testing new generation algorithms and validating biophysical variable products. Rather than being aimed at a specific sensor program, this project allows the inter-comparison between sensors and algorithms (Weiss et al., 2001).

The MODIS land discipline team (MODLand) uses field and tower measurements, fine resolution (less than 10 m Instantaneous Field of View, IFOV), and high resolution (from 10 to 30 m IFOV) imagery from airborne and satellite sensors, to compare with the MODIS 1 km product (Justice et al., 2000). However, the uncertainty assessment of these products is not straightforward. The 1-km resolution of the MODIS LAI product significantly exceeds the plot size typically used for LAI and FPAR field measurements. Thus, a procedure is needed to correlate the scale of the LAI measurements to the scale of the MODIS pixels using high-resolution imagery. Except for a few studies directly addressing validation such as comparing albedo (Lucht et al., 2000; Stroeve et al., 2001), Bidirectional Reflectance Distribution Function (BRDF) (Lewis et al., 1999; Hautecoeur & Leroy, 2000), and LAI (Weiss et al., 2001) with field data, there have been a limited number of comparisons between ground-based and satellite-derived land variables. The paucity of such work to date is an indication of the logistic and practical difficulties in the comparison. Validation work still requires accurate and efficient procedures to assess the uncertainties of moderate resolution satellite products.

This paper, which is divided into two parts, attempts to assess the uncertainty of the MODIS LAI product via comparisons with ground and high-resolution satellite data, and provide guidance for field data collection and sampling strategies. Part I, presented here, proposes a region or patch-based comparison method, which can be implemented on a routine basis, and addresses the issue of spatially scaling ground-based point measurements to the scale of satellite observations. In lieu of using MODIS data, we provide comparisons of validated 30 m ETM+ LAI retrievals to those derived from the 250-, 500-, and 1000-m resolutions of simulated MODIS data (MODIS data were largely unavailable during the period of campaigns as it was too soon after launch). The estimation of uncertainty of MODIS LAI data from SAFARI 2000 wet season campaign is the main task in this paper. Part II applies hierarchical analysis to data from campaigns at the Maun (Botswana), Harvard Forest (USA) and Ruokulahti Forest (Finland) to obtain multiscale variation in the LAI data, and proposes a ground sample collection strategy.

## 2. SAFARI 2000 wet season Kalahari Transect campaign

SAFARI 2000 is an organizational umbrella for various studies, which together should improve understanding of the sources, transformations, dynamics, sinks and impacts of atmospheric aerosols in Southern Africa (Swap & Annegarn, 1999). A major component of SAFARI 2000 is remote sensing research and validation with NASA EOS data products (Privette et al., 2002). An international group of researchers completed an intensive field campaign in Botswana and Zambia between February 28 and March 18, 2000. These dates coincided with the first weeks of MODIS Earth view because of launch delay. The activity was the second of four planned intensive campaigns of SAFARI 2000. The field sites are located along the International Geosphere–Biosphere Program (IGBP) Kalahari Transect (KT). The KT extends over a large rainfall gradient (200 to 1000 mm/year mean annual rainfall) in an area of uniform soils, the Kalahari sands. The vegetation extends from equatorial forest to subtropical, arid shrubland of the Kalahari desert (Dowty et al., 2000).

We collected field data to validate the MODIS LAI algorithm. Ground measurements of LAI, leaf hemispherical reflectance and transmittance and canopy transmittance were taken using the LAI-2000 plant canopy analyzer, AccuPAR ceptometer, LI-1800 portable spectroradiometer

and ASD handheld spectroradiometer during the period from March 3 to March 18, 2000, in Botswana. LAI was intensively measured at four different sites, Pandamatenga, Maun, Okwa and Tshane (from north to south in Botswana), where the vegetation ranged from moist closed woodland to arid grasslands with scattered shrubs.

### 2.1. Sampling methods

At each of the four sites, data were collected within a $1 \times 1$ km region on three transects of 750 m and on a $250 \times 300$ m grid (Fig. 1). For the transects, measurements were made along three straight, parallel lines, "B", "A", and "N" from south to north, each of 750 m in length. We took LAI measurements at 25-m intervals from west to east, for a total of 31 sample points on each 750-m transect. Each sample point was labeled as A375W, A00, A375E... and so on. "A00" represents the middle sample point on the "A", and "A375W" represents the sample point located 375 m west of A00. We used a Garmin II+ Global Positioning System (GPS) receiver in "averaging" mode (allows more precise determination), which had a typical uncertainty of about 12 m, for sample point geoferencing. The GPS system still had artificial noise during the campaign. At a minimum, we collected GPS points at the ends and middle of each transect, i.e., at three points for each transect. The points in-between those geolocated points were determined with a Suunto KB-20 Handbearing com-

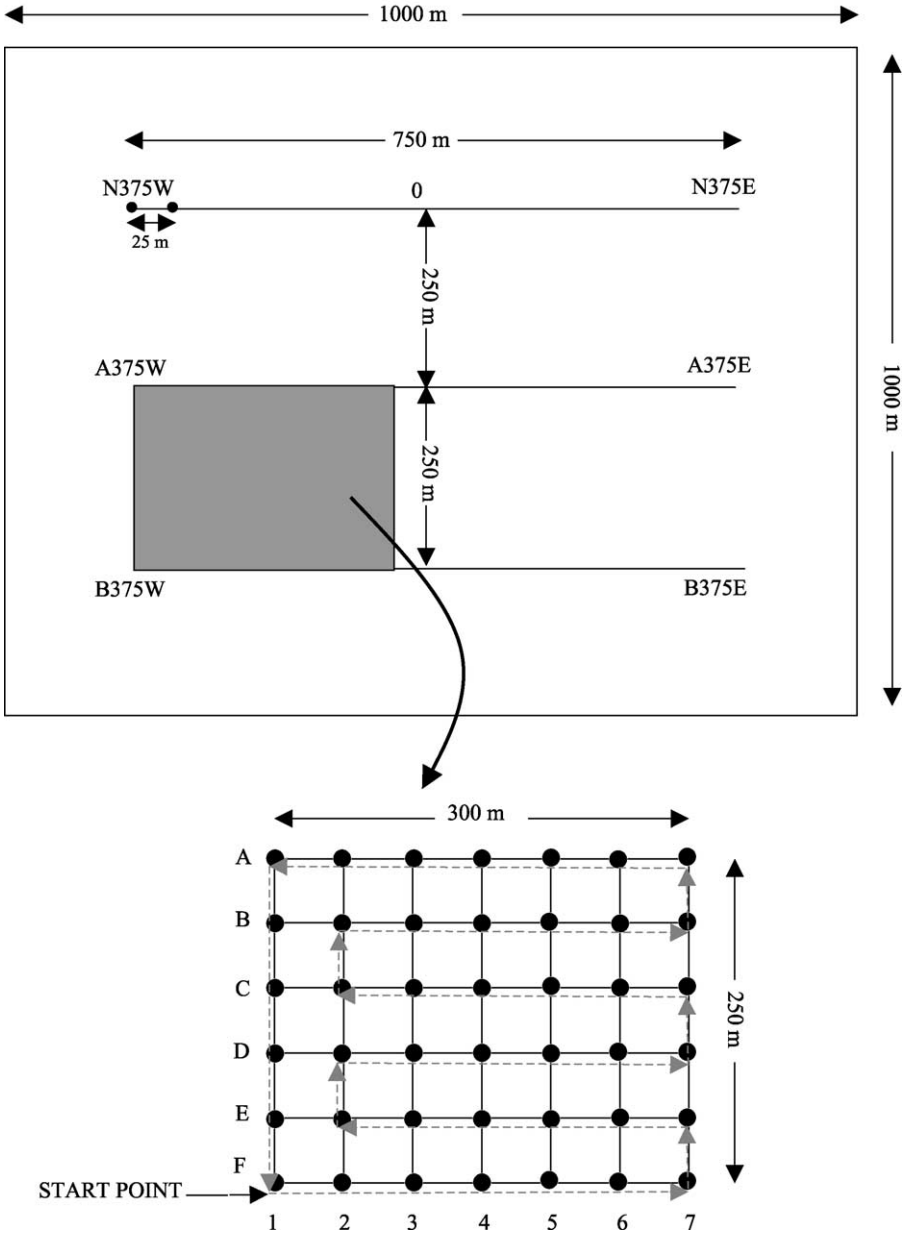


Fig. 1. Sampling scheme of SAFARI 2000 wet season Kalahari Transect (KT) campaign.

pass and the Haglof Distance Measuring Equipment (DME) 201, calibrated on-site and accurate to 1%.

On the grid, measurements were taken at a 50 × 50 m resolution in a rectangular area, located at the southwest corner of the 1 km$^2$ site. There were 6 east–west oriented lines (300 m in length) and 7 south–north oriented lines (250 m in length) for a total of 42 sample points. Each line was named A, B, C, D, E, and F from north to south. There were 7 sample points, numbered 1 to 7 from west to east, on each line (A, B, C, D, E, or F). Therefore, we named the sample points in this rectangular area as F1, F2, ..., F7 ...and so on. The measurements were taken as follows: from F1 to F7, E7 to E2, D2 to D7, C7 to C2, B2 to B7, A7 to A1, and then to E1.

At the Maun site, we also collected another 34 measurements around the scaffolding tower (19.91641°S, 23.5594°E), set up by the Max Plank Institute. This tower was located at 1-km northwest of the 1-km intensive study area. The sampling method was similar to the grid measurement. The vegetation type was savanna. We labeled this site as T (tower). This tower site contained older, sparser vegetation. We primarily measured this Tower site in order to compare its LAI value with our 1-km study area's LAI data, and wanted to make sure the vegetation at both sites characterized with the same methods and instruments. This facilitated relating the LAI differences to structural and vegetation type differences.

### 2.2. LAI measurements

We measured LAI using the LAI-2000 plant canopy analyzer, which consists of a LAI-2070 control unit and a LAI-2050 sensor head. The control unit has connectors for two sensor heads, two connectors for other LI-COR sensors, and a connector for RS-232 communication. The sensor head projects the image of its nearly hemispheric view onto five detectors arranged in concentric rings (approximately 0–13°, 16–28°, 32–43°, 47–58°, 61–74°). Radiation above 490 nm is not measured (LI-COR INC., 1992).

Three LAI-2000 units were used in this campaign, two in the field, and the other in an open space as a reference for incident radiation. The two sample units were calibrated against the reference unit under overcast conditions or shortly before sunset, prior to field measurements. The calibration procedures are given in the LAI-2000 Plant Canopy Analyzer Instruction Manual, Chapter 4-1 (LI-COR INC., 1992). The reference unit was set in remote logging mode at a sampling frequency of one per 60 s.

The LAI-2000 measures attenuation of diffuse sky radiation at five zenith angles simultaneously. LAI measurements were done mostly right before and after sunset. Some measurements in Pandamatenga and Maun were taken during dawn. In Tshane, one set of measurements was taken in the afternoon under overcast conditions.

All the measurements were taken by holding the sensors opposite to the direction of the sun. A 90° mask was used in Pandamatenga and Maun to prevent interference caused by the operator's presence. A 270° mask was used in Okwa and Tshane because of the heterogeneous distribution of shrubs and trees on the grassland. The same mask was used for the reference sensor as well.

From beneath a canopy, the sensor's potential field of view resembles an inverted cone whose radius ($r$) is roughly three times the canopy height. The sensor's view limit is 74°, the tangent of which is 3.48. A value of 3 serves as a working number, because of the reduced probability that foliage at the edge of the sensor's field of view will be significant (LI-COR INC., 1992). Therefore, the measured resolution (area) of each site is

$$\text{Area} = \pi r^2 = \pi(3h)^2, \quad (1)$$

where $h$ is the tree or plant height. The woody plant height on the Kalahari Transect was measured by Scholes et al. (in press) during this campaign. The average plant height at the four sites (Scholes et al., in press) is listed in Table 1. The actual measured area was three fourths of the total area in Pandamatenga and Maun, and one fourth in Okwa and Tshane. The percentage overlap between two adjacent measurements is also listed in Table 1.

## 3. Heterogeneity of measured LAI at the SAFARI 2000 sites

### 3.1. Statistical analysis of means

Histograms of measured LAI along the transects and the grid are shown in Fig. 2. The mean and standard deviation are given in Fig. 3. One immediate question concerns the similarity of the grid and transect measurements. Are they sampling the same population? A $t$-statistic was used to test the null hypothesis that the mean values of two groups are

Table 1
Plant height (Scholes et al., in press) and LAI-2000 measured area

| Site | Height (m) | Radius (m) | Total area (m$^2$) | Actual area (m$^2$) | Overlap at transect (%) | Overlap at grid (%) |
|---|---|---|---|---|---|---|
| Pandamatenga | 11.4 | 34.2 | 3674.53 | 2755.89 | 39.36 | 0 |
| Maun | 6.0 | 18 | 1017.88 | 763.41 | 0 | 0 |
| Okwa | 2.2 | 6.6 | 136.85 | 34.21 | 0 | 0 |
| Tshane | 3.7 | 11.1 | 387.07 | 96.77 | 0 | 0 |

Transect measurements were taken at 25-m intervals, while grid measurements were taken at a 50 × 50 m resolution.

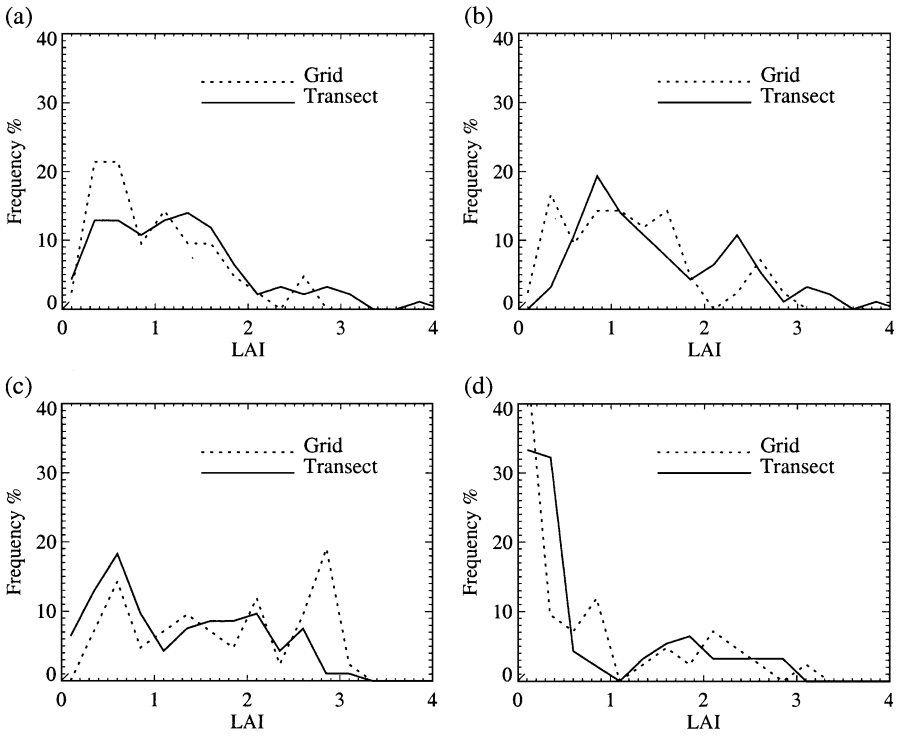


Fig. 2. Histograms of transect and grid LAI measurements at the four SAFARI 2000 wet season campaign sites: (a) Pandamatenga, (b) Maun, (c) Okwa, and (d) Tshane.

equal. The *t*-test results (Table 2) indicate that the means of the transect and grid measurements are statistically different in Maun and Okwa at $p<0.05$ and Pandamatenga at $p<0.10$. Tshane, on the other hand, shows a very high probability of equal means. These results indicate that LAI in three of the four sites are not spatially uniform. For the tower site (T) at Maun, the mean LAI value, 1.04, is smaller than those from transect and grid measurements at Maun.

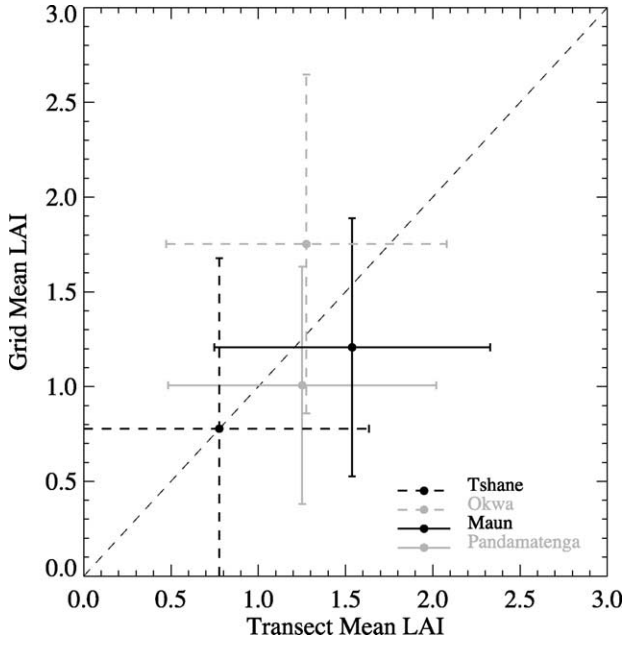


Fig. 3. Comparison between transect and grid LAI measurements at Pandamatenga, Maun, Okwa, and Tshane. The dots and error bars represent means and standard deviations, respectively.

### 3.2. Semivariance analysis

The spatial heterogeneity of measured LAI can be quantitatively described by estimating the spatial dependence of LAI within each site. A useful measure of spatial variation in the values of a variable $Z$ is the semivariance, which is half the average squared difference in $Z$ values between pairs of sample points. For a stationary and isotropic spatial process, the semivariance $\gamma$ in $Z$ values between all pairs of points $Z(x)$ and $Z(x+h)$ separated by distance $h$ (referred to as "lag") can be estimated from sample data (Woodcock, Collins, & Jupp, 1997),

$$\gamma(h) = \frac{1}{2N(h)} \sum_{N(h)} [Z(x+h) - Z(x)]^2. \quad (2)$$

Here $N$ is the number of pairs of sample points $(x, x+h)$ separated by distance $h$.

Table 2
*t*-Test of the means of the transect and grid LAI measurements

| Site name | | | |
|---|---|---|---|
| Pandamatenga | Maun | Okwa | Tshane |
| 0.0725 | 0.0269 | 0.0023 | 0.9952 |

The null hypothesis is that the LAI means of the two groups are equal. Here, $p$ values are given.

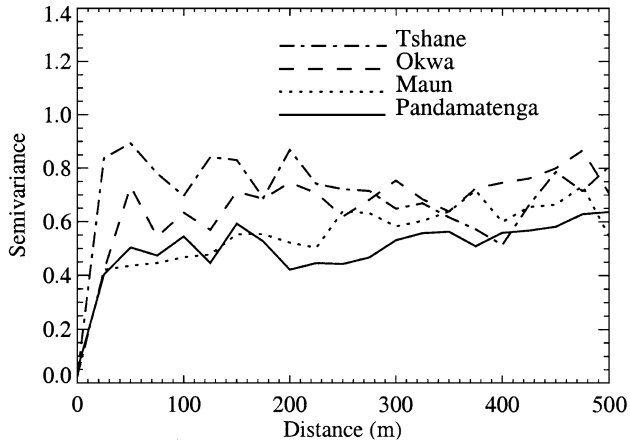


Fig. 4. Semivariograms of field measurements at Pandamatenga, Maun, Okwa, and Tshane.

The key to investigation of the semivariance is the construction of a semivariogram, which is a plot of the semivariance, $\gamma(h)$, as a function of distance $h$. There are several important features noteworthy in a sample semivariogram. At relatively short distance $h$, the semivariance is small, but increases with distance between pairs of sample points. At a distance referred to as "range", the semivariance levels off to a relatively constant value, referred to as the "sill". This implies that beyond this range, $Z$ values are no longer spatially correlated. Within this range, $Z$ values are more similar when the pairs of sample points are closer together. The semivariograms of LAI (Fig. 4) at the four sites show a similar structure, with a small range of less than 50 m. This means that the LAI values among the sample points are not spatially related except for direct neighbors along the transects which are 25 m apart, indicating a high level of heterogeneity in the spatial distribution of LAI. This effect is also evident in simple plots of the transect LAI measurements (Fig. 5). We conclude that the variance in LAI within these sites is large and little spatial structure exists in measurements collected at 25-m intervals.

## 4. Validation of the MODIS algorithm LAI at Maun

Our objective here is to validate 1-km$^2$ LAI values derived from MODIS data through comparison with field measurements. The first challenge is how to validate coarse resolution MODIS LAI with fine resolution measurements from the four 1-km$^2$ sites, each with an area equivalent to only one MODIS pixel, but imperfectly aligned with the pixel. In total, there are only four pairs of pixels at 1-km$^2$ resolution between the field measurements and MODIS data. In addition, if the spatial registration is not accurate,

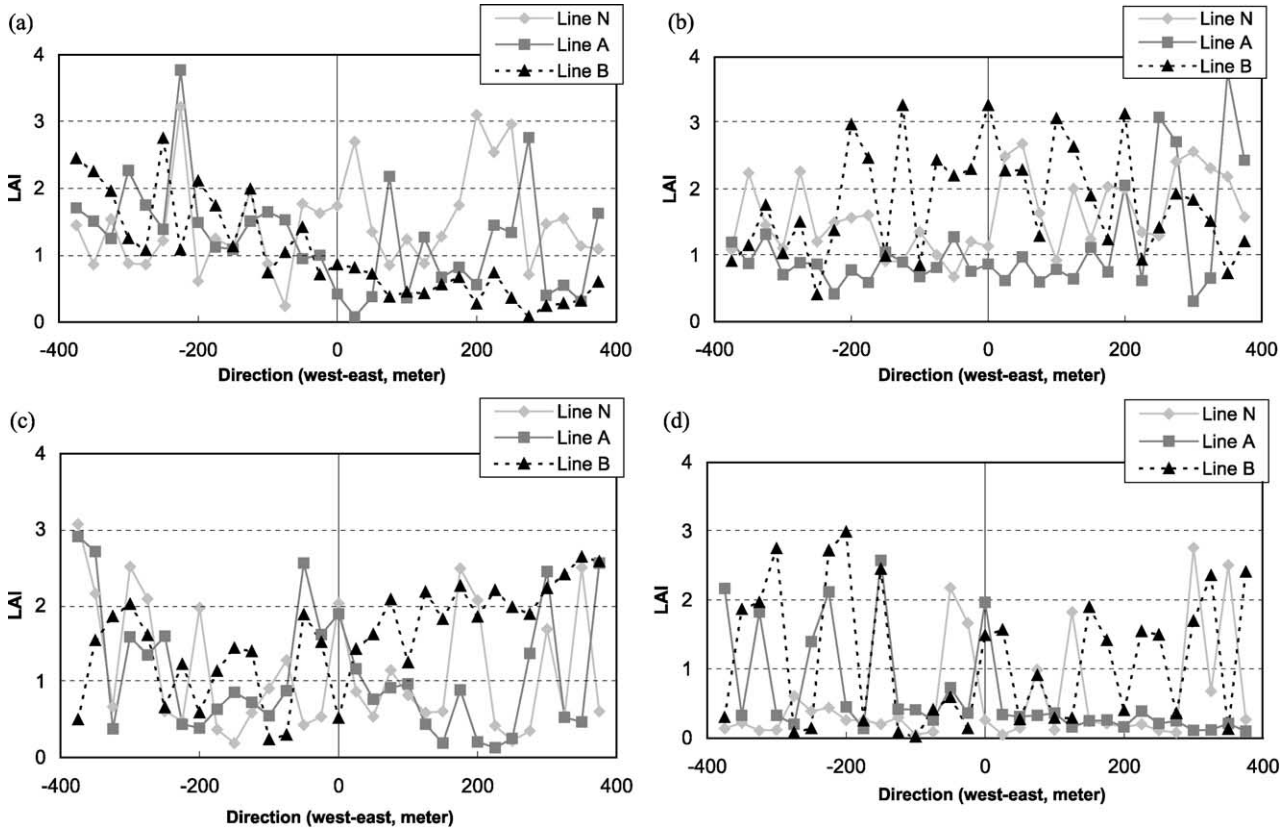


Fig. 5. LAI measurements along the transects from the sample points located 375 m west of the middle sample points to those located 375 m east. (a) Pandamatenga, (b) Maun, (c) Okwa, and (d) Tshane.

some of the field measurements may fall out of the 1-km$^2$ MODIS pixel, and this makes the comparison less reliable. Therefore, we propose to first validate and produce a LAI map of a 10 × 10 km region from ETM+ data based on our field measurements. Using this ETM+ LAI map, we can validate the MODIS LAI product. In view of the large amount of work associated with field and satellite data processing, classification, atmospheric correction, geo-registration, etc., we use data from the Maun site only to illustrate our strategy for validation of the MODIS LAI product.

### 4.1. The MODIS LAI and FPAR algorithm

For each of the land pixel, the operational MODIS algorithm ingests up to seven atmosphere-corrected surface spectral bi-directional reflectance factors (BRFs) and their uncertainties and outputs the most probable values of LAI, FPAR and their respective dispersions. The theoretical basis of the algorithm is given in Knyazikhn, Martonchik, Myeni, Diner, and Running (1998) and the implementation aspects are discussed in Knyazikhin et al. (1999). A Look-Up Table (LUT) method is used to achieve inversion of the three-dimensional radiative transfer problem (Myneni et al., in press).

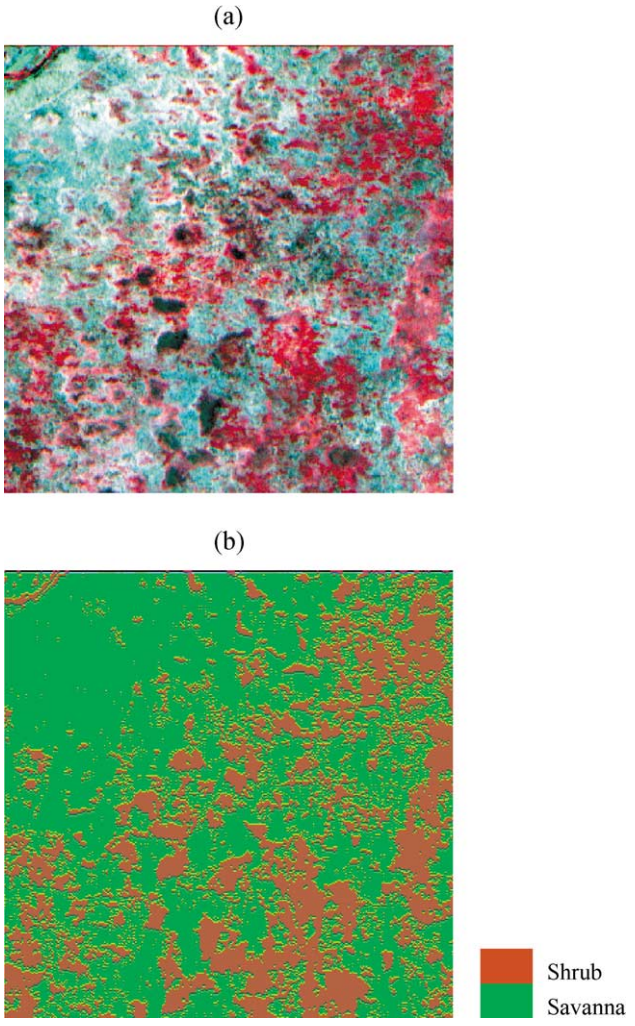


Fig. 6. (a) Color RGB image from Bands 4, 3 and 2 of a 10 × 10 km region of the Maun site from an ETM+ image. (b) Vegetation classification map for the 10 × 10 km region.

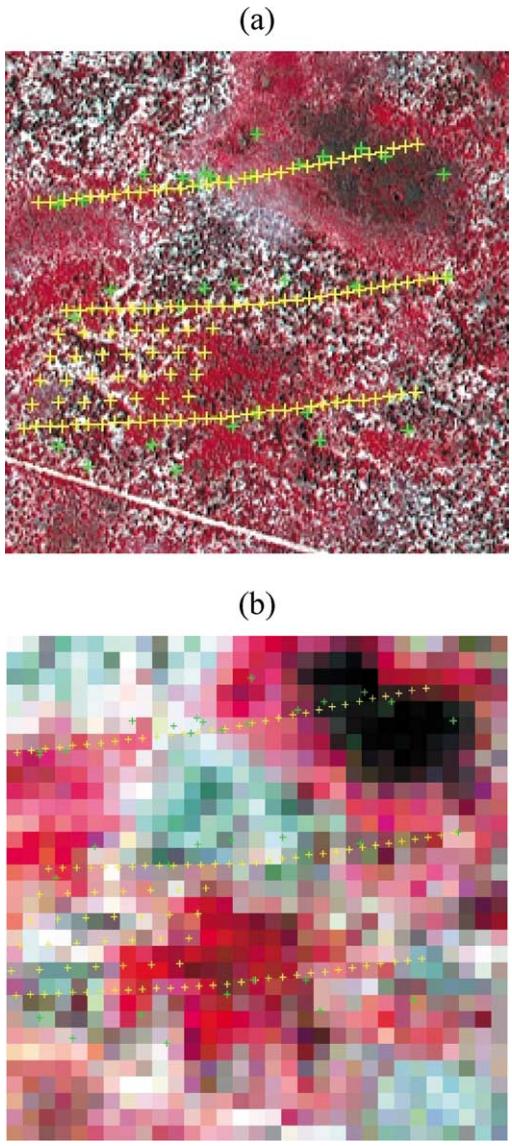


Fig. 7. Color RGB image from Bands 4, 3 and 2 of a 1 × 1 km region of the Maun site. Panel (a) is IKONOS data and panel (b) is ETM+ data. Yellow "+" represents sampling points, and green "+" represents the positions where photographs were taken.

### 4.2. Selection of a 10×10 km ETM+ region

We selected a subset of a Landsat ETM+ image from April 3, 2000 (Fig. 6a), and a subset of an IKONOS image from March 30, 2000, with the point A00 of the Maun site as the central point. The ETM+ and IKONOS subsets have spatial resolutions of 30 and 4 m, respectively, and cover a 10 × 10 km region. Both images were in the Universal Transverse Mercator (UTM) projection and were corrected

for atmospheric effects using the standard SMAC method (Rahman & Didieu, 1994; Häme et al., 2001). The IKONOS image was mainly used to help identify features and regions. We also have 33 photographs with GPS navigation readings. The ETM+ subset was classified into vegetation classes, shrubs and savanna (Fig. 6b), using an unsupervised classification approach, with the aid of field photographs and an IKONOS image. Savanna and shrubs occupy 65% and 35% of the total area, respectively.

### 4.3. Validation of 1×1 km ETM+ LAI

We now focus on a 1 × 1 km area in the ETM+ subset, with the point A00 as the central point. This region corresponds to where the field measurements were taken in Maun. We ran the MODIS LAI algorithm using ETM+ surface reflectances at RED and NIR band to produce ETM+ LAI fields, and compared the retrieved fields with *in situ* measurements at 30-m resolution.

#### 4.3.1. Image segmentation

The problem is how to compare the field and ETM+ LAI data? A pixel-by-pixel comparison is not feasible for several reasons. First, the area (34–2756 $m^2$) measured with LAI-2000 (Table 1) is either larger or smaller than the resolution of the ETM+ (900 $m^2$). Therefore, the individual LAI measurements are not representative of 30 m ETM+ pixels, and the ground measurements and ETM+ pixels cannot be reliably matched. Second, the GPS readings at the measurement sites are not accurate. The measurements and photographs did not give the same GPS readings (accurate GPS estimates were possible only 4 months after the campaign). Third, because of the high variance of LAI measurements over short distances, there are some errors associated with field measurements and mismatch between measurements and image pixels. It is essential to identify multi-pixel patches in the image data to validate the algorithm.

In the analysis of remotely sensed imagery, pixels are assumed to be representative samples of objects in the scene. When pixels are large relative to ground objects, individual pixels often cover parts of two or more objects, resulting in mixed pixels, and the effectiveness of analysis is undermined (MacDonald & Hall, 1980; Woodcock & Strahler, 1987). Similarly, when pixels are small relative to the objects, internal variance of the objects adversely affects the analysis (Cushnie, 1987; Markham & Townshend, 1981). The ideal situation is when the elements of analysis in the image correspond to homogenous objects in the scene (Woodcock & Harward, 1992). The objective of image segmentation is to partition the image into a set of regions, which correspond to homogeneous objects in the ground scene and will serve as the basis of further analysis (Beaulieu & Goldberg, 1989). Therefore, the spectral attributes of regions defined via segmentation may more accurately be grouped into categories than the pixels comprising the region when taken singly (Woodcock & Harward, 1992).

We use a multiple-pass region-based algorithm named nested-hierarchical scene model (Woodcock & Harward, 1992) segmentation procedure to generate groups of ETM+ pixels, or regions, corresponding to patches of vegetation to serve as the basis of validation of the MODIS LAI algorithm. The multiple-pass approach allows slow and careful growth of regions while inter-region distances are below a global threshold. Past the global threshold, a minimum region size parameter forces development of regions in areas of high local variance. Maximum and viable region size parameters limit the development of undesirably large regions (Woodcock & Harward, 1992). The advantage of this model is that it can recognize different scales of objects in a scene. Each level in the hierarchy is nested, or composed of objects or categories of objects from the preceding level, and different objects may have distinct attributes (Woodcock & Harward, 1992).

Fig. 7a displays the IKONOS image, combined with Bands 4, 3, and 2. Fig. 7b shows the same area, but with the coarser resolution ETM+ image, of which individual pixels are visible. The sampling points of measurements (yellow "+") and the positions of photographs taken (green "+") are also shown in Fig. 7a and b. From a simple visual examination of these images, it is apparent that the landscape is heterogeneous and patchy, and the LAI measurements were made on different patches. The segmentation algorithm grouped pixels into patches based on their spectral similarity and adjacency, with Bands 3, 4 and 5 of the ETM+ image as inputs. The resulting map (Fig. 8) yielded patches corresponding to identifiable features in the landscape. There are 15 patches in total. Most of the measurements fall in patches 3, 5, 6, 7, 8, 9, 10 and 12. According to the land cover map (Fig. 6b), patches 3, 5, 6 and 10 are mostly shrubs, and patches 7, 8, 9, 12 are mostly savanna. The LAI measurements were grouped by patch, excluding points located at patch boundaries, because patch membership was ambiguous. Patches 7 and 8 were merged, because

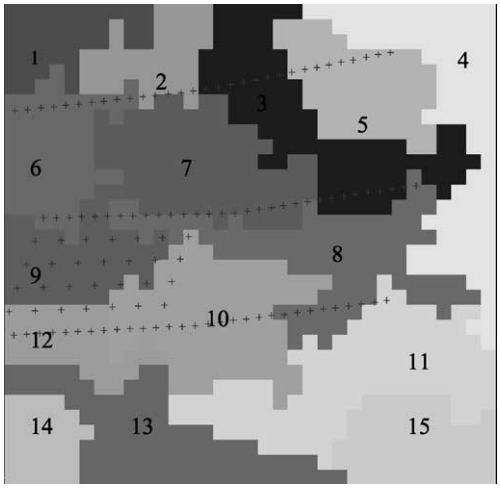


Fig. 8. Map of a 1 × 1 km region at Maun using the segmentation procedure described in the text. Patches 1, 2, 4, 7, 8, 9, 12, 13 and 15 are savanna patches. Patches 3, 5, 6, 10, 11, and 14 are shrub patches.

Table 3
*t*-Test of the LAI means of different regions

| Class type | Region number | Region number | | | | | | | |
|---|---|---|---|---|---|---|---|---|---|
| | | 3 | 5 | 6 | 10 | 7+8 | 9 | 12 | Tower |
| Shrub | 3 | 1.0000 | | | | | | | |
| | 5 | 0.3614 | 1.0000 | | | | | | |
| | 6 | 0.4108 | 0.0108 | 1.0000 | | | | | |
| | 10 | 0.7928 | 0.4862 | 0.2412 | 1.0000 | | | | |
| Savanna | 7+8 | 0.0241 | 0.0003 | 0.0713 | 0.0050 | 1.0000 | | | |
| | 9 | 0.0993 | 0.0035 | 0.2539 | 0.0349 | 0.5922 | 1.0000 | | |
| | 12 | 0.2747 | 0.0220 | 0.7243 | 0.1259 | 0.1722 | 0.4569 | 1.0000 | |
| | Tower | 0.0085 | 0.0001 | 0.0382 | 0.0010 | 0.8112 | 0.4309 | 0.0901 | 1.0000 |

The null hypothesis is that the LAI means of the two groups are equal. Here, $p$ values are given.

most of the measurements on the line "A" are located at the edge of patches 7 and 8, both of which were savanna. There is one more savanna patch "T", as mentioned before. Thus, there are eight groups (patches) of LAI measurements, with four of savanna and four of shrubs. We calculated the mean LAI for each group, and use the *t*-statistic to test whether the means of any two patches are equal. The results (Table 3) show that groups from the same land cover class generally have a higher probability of equal mean LAI value than those of different classes, which are always significantly different, except for group 6 and group 12 (Table 3). Image segmentation thus helped in regrouping the measurements.

### 4.3.2. *Validation of the MODIS LAI algorithm at 30-m resolution*

To test the MODIS LAI algorithm at 30-m resolution, it was executed (Knyazikhin, Martonchik, Diner, et al., 1998; Knyazikhin, Martonchik, Myneni, Diner, Running, 1998) for each pixel in the ETM+ image using Band 4 (NIR) and Band 3 (RED) reflectance data, and the patch map to define

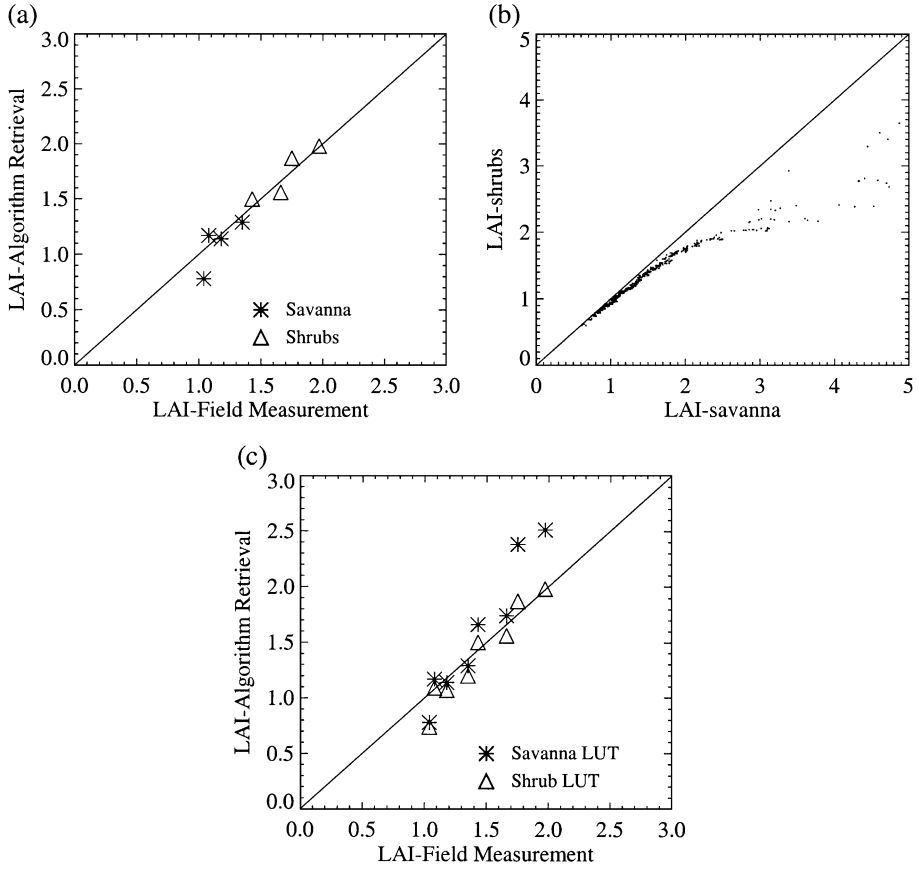


Fig. 9. (a) Patch-by-patch comparison of field measurements and MODIS algorithm based LAI from 30-m resolution ETM+ data at Maun. (b) Pixel-by-pixel comparison of retrieved LAI of all pixels using savanna Look-Up Table (LUT) ($x$-axis) and shrubs LUT ($y$-axis). This figure shows that if we define all pixels in one scene as savanna only or shrubs only, savanna LUT generally gives a higher LAI value than shrub LUT. (c) Patch-by-patch comparison of LAI retrievals from savanna and shrub LUT with field measurements.

biome type. Pixels from patches 3, 5, 6, 10 were retrieved with the shrub Look-Up Table (LUT), and pixels from patches 7, 8, 9, 12 with the savanna LUT. The mean values of the retrieved and measured LAI of each patch are shown in Fig. 9a. Most of these are along the 1:1 line. The savanna patches have LAI values consistently lower than the shrubs. The consistency between LAI retrievals and field measurements indicates satisfactory performance of the algorithm.

To investigate the effect of misclassification on LAI retrievals, the LAI values of all pixels were retrieved using the savanna LUT only and the shrub LUT only. Fig. 9b is the scatter plot of these retrievals. For a pixel with the same surface reflectance, the savanna LUT generally gives a higher LAI value than the shrub LUT. The difference is small for pixels with LAI values less than 2, but larger for higher values. In this case most pixels have LAI values less than 2, with a mean of 1.32 for shrub LUT retrievals and 1.45 for savanna LUT retrievals. For an individual patch, however, the misclassification effect can be larger. Fig. 9c shows the comparison of patch mean LAI of the measurements and retrievals using the different LUTs. If the shrub pixels are retrieved using the savanna LUT, the patch mean LAI will be higher than the measurements. The difference can be as high as 0.5 LAI for patches 5 and 10. Therefore, it is essential to

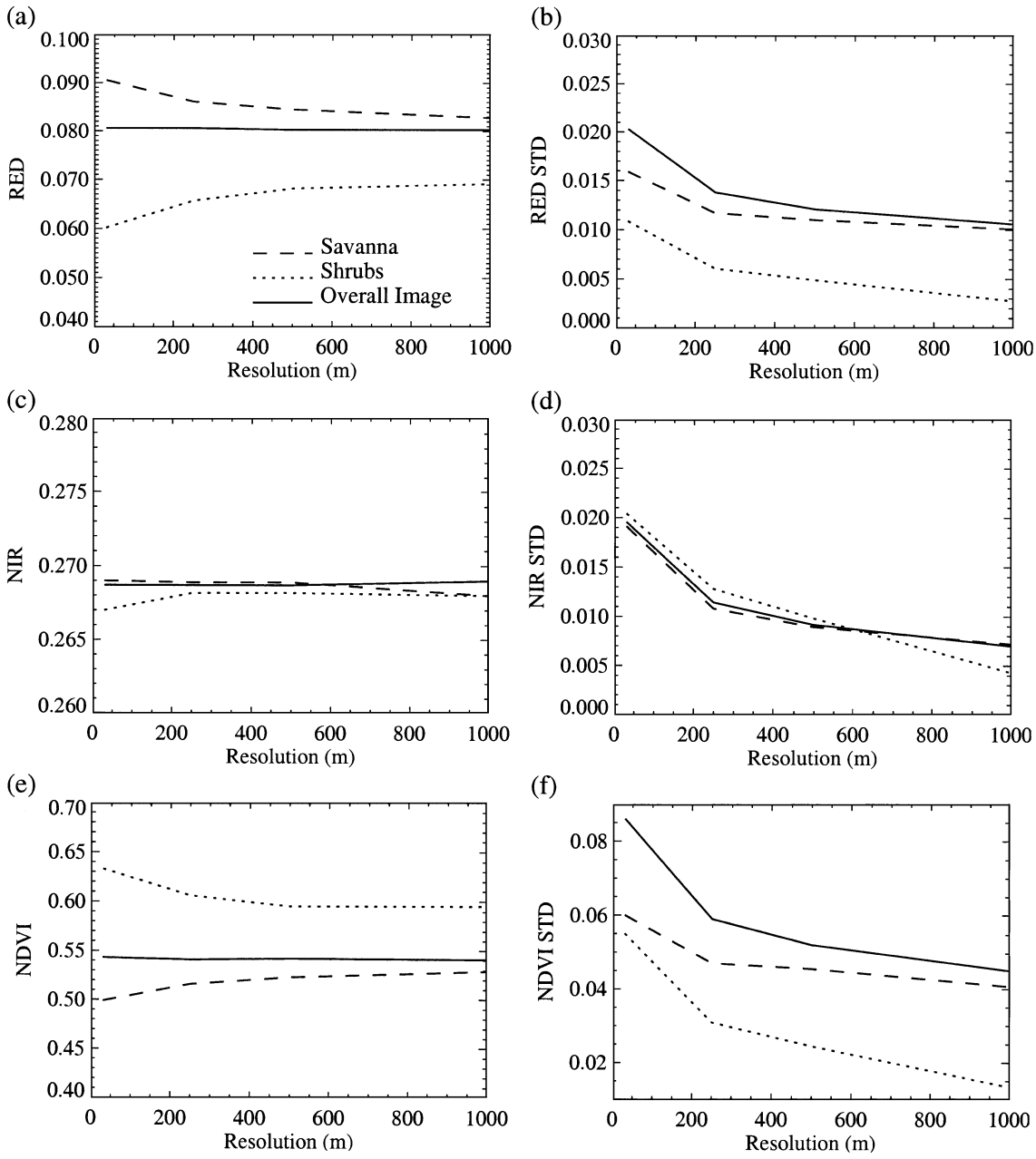


Fig. 10. The mean and standard deviation (STD) of RED reflectance, NIR reflectance, and NDVI as a function of spatial resolution: (a) mean of RED, (b) STD of RED, (c) mean of NIR, (d) STD of NIR, (e) mean of NDVI, and (f) STD of NDVI.

identify the cover type accurately for validation and operational mapping of LAI.

## 5. Resolution effects on MODIS LAI retrievals

A common approach to study the effects of resolution between fine and coarse resolution results is to compare data from sensors with varying resolutions or to aggregate fine resolution data to larger cell sizes (Chen, 1999; Pax-Lenney & Woodcock, 1997; Tian et al., in press). The SAFARI 2000 wet season campaign was conducted 2 months after Terra was launched. Unfortunately, this campaign period was during the first weeks of MODIS operation, and there were no MODIS reflectance data and products during that period. Therefore, we created coarse resolution data from the 30-m resolution ETM+ data. The ETM+ data from Bands 3 and 4 in the $10 \times 10$ km study area were spatially degraded to generate data of 240-, 480-, and 960-m resolutions. The program used to degrade the ETM+ image was developed as part of an effort to simulate the spatial resolution of MODIS-N sensor from ETM+ imagery using a convolution algorithm developed by Barker et al. (1992). The ETM+ data are forward Fourier transformed, multiplied by the transfer function of a Gaussian blur filter and then inverse Fourier transformed. The resulting output array is reduced to the appropriate size through nearest neighbor re-sampling (Barker et al., 1992; Pax-Lenney & WoodCock, 1997). The aggregated 240-, 480-, and 960-m resolutions correspond closely to MODIS resolutions of 250, 500, and 1000 m, which are used through the remainder of the text. The spatially degraded data for each band, however, retain the ETM+ spectral bandwidths. At coarse resolution, we label the class type of each pixel by majority rule.

### 5.1. Relation between changes in reflectance and spatial resolution

To investigate the effect of changes in resolution on MODIS LAI retrievals, an understanding of the relation between changes in reflectance and spatial resolution is needed. Fig. 10 shows variations in the mean and standard deviation (STD) of RED and NIR reflectances, and NDVI, as a function of spatial resolution. NDVI was calculated directly from coarse resolution reflectance data.

Without consideration of the land cover type, the overall mean values (RED, NIR, NDVI) of the image show little or no change with resolution. However, the mean values for different classes change quickly. For a class with a higher (lower) mean value, its mean value decreases (increases) as

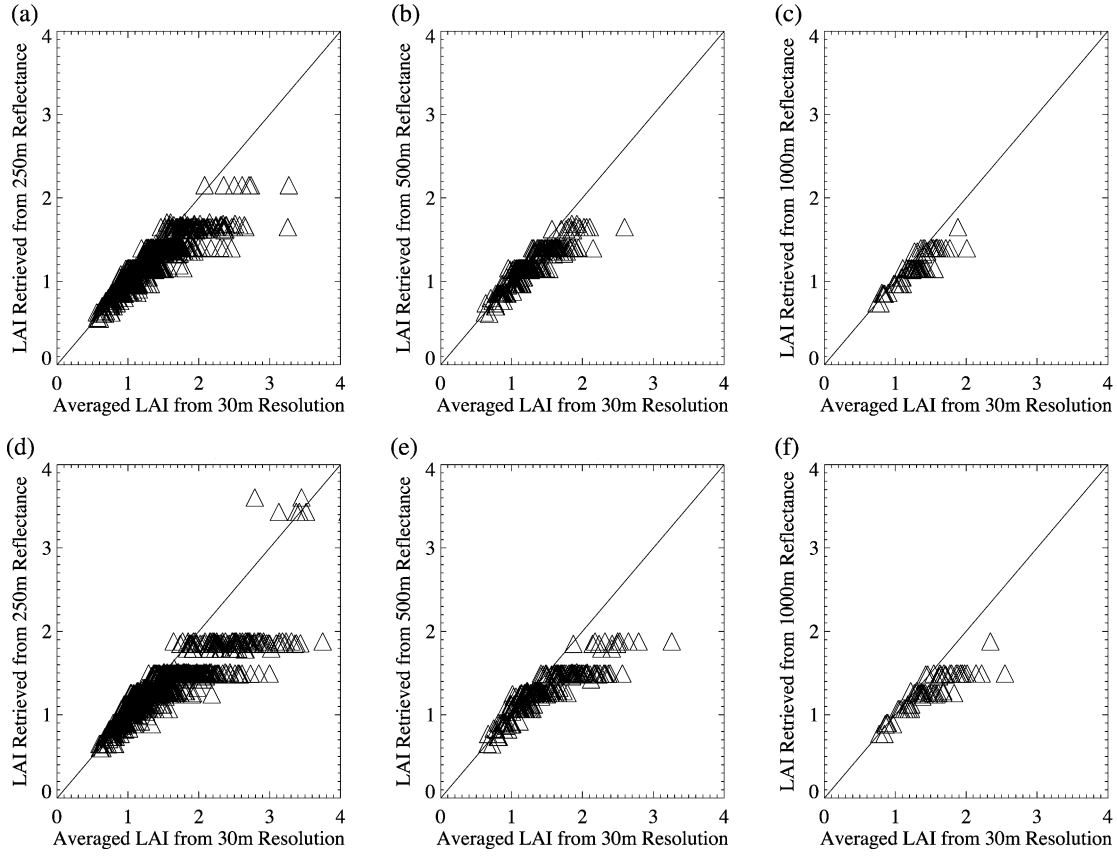


Fig. 11. Pixel-by-pixel comparison of LAI values averaged from 30-m resolution and retrieved directly from reflectance at resolution of (a) 250 m using shrub look-up table (LUT) only, (b) 500 m using shrub LUT only, (c) 1000 m using shrub LUT only, (d) 250 m using savanna LUT only, (e) 500 m using savanna LUT only, and (f) 1000 m using savanna LUT only.

resolution decreases, with the overall mean value remaining invariant. That is, the difference in the mean values between savanna and shrubs becomes smaller. The decrease in the STD with coarser resolution is obvious. We conclude that spatial aggregation results in a decrease in the variance of the data and a smaller discrepancy in mean reflectance between different classes. This effect occurs because the number of mixed pixels in the image and the degree of spatial mixture within pixels increase as the spatial resolution becomes coarser. As a result, there will be some loss of spectral separability between the land cover classes defined at finer spatial scales.

### 5.2. Non-linearity in LAI retrievals from one land cover type

The goal of scaling is to establish values of LAI retrieved from coarse resolution sensor data to equal the arithmetic average of LAI values retrieved independently from fine resolution sensor data (Hall, Huemmrich, Goetz, Sellers, & Nickeson, 1992; Tian et al., in press). Coarse resolution LAI can be derived by two methods. First, LAI values are generated from ETM+ reflectance data using the MODIS algorithm at 30-m resolution, and then averaged over space to estimate LAI at coarse resolutions (method 1). This is the correct way. Second, LAI values are generated directly from the simulated coarse resolution reflectance data using the same MODIS algorithm (method 2). For each of the coarse resolution pixels, the following equation quantifies the difference in LAI (DL) retrievals between method 1 and method 2.

$$\mathrm{DL} = (\mathrm{LAI}_{\mathrm{method\ 1}} - \mathrm{LAI}_{\mathrm{method\ 2}})/\mathrm{LAI}_{\mathrm{method\ 1}}. \quad (3)$$

If DL is positive, method 2 underestimates the LAI value; otherwise, method 2 overestimates the LAI value. Theoretically, any algorithm will not over- or underestimate the LAI value if the input data are homogeneous, or if the algorithm is linear with respect to surface reflectance data.

For simplicity, assume that there is only one land cover type in the 10 × 10 km image, either savanna or shrubs. This assumption eliminates the effect of mixture of land cover types. The overall mean reflectance and NDVI do not change appreciably as the resolution decreases, as illustrated in Fig. 10. Does the overall mean LAI not change either? Fig. 11 and Table 4 compare the LAI retrievals from method 1 and method 2. The mean DL values are always positive, that is, the LAI values are underestimated when retrieved from coarse resolution data. The algorithm underestimates more when using savanna LUT than when using shrub LUT given the same reflectance values. The underestimation is larger as spatial resolution decreases.

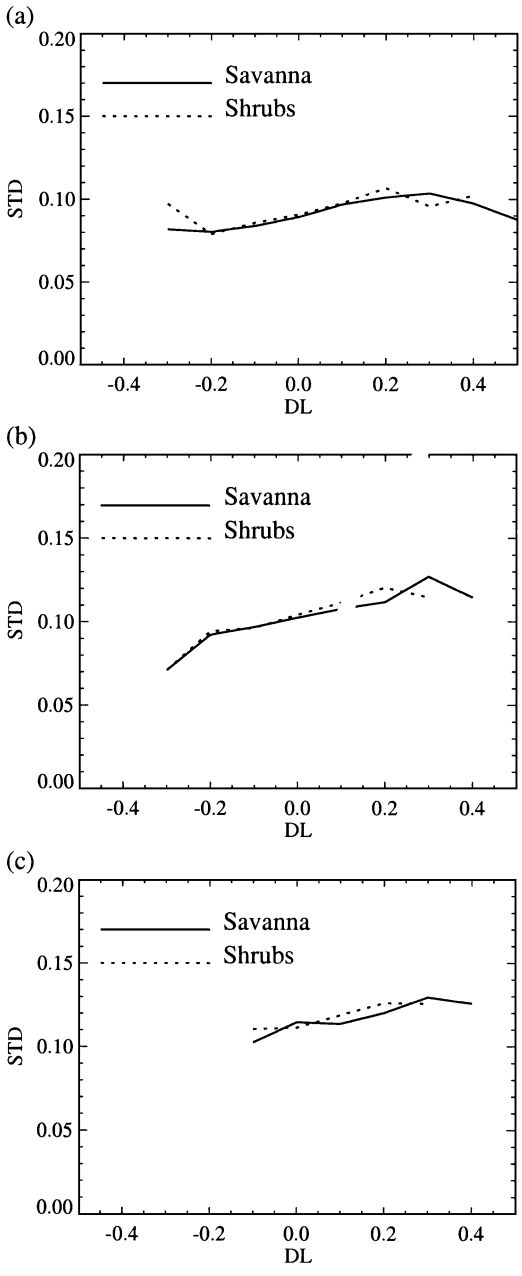


Fig. 12. Overall standard deviation as a function of the difference in LAI (DL) between averages from 30 m resolution and retrievals directly from reflectance at (a) 250 m, (b) 500 m, and (c) 1000 m resolution.

Table 4
Means of difference in LAI (DL) retrievals between method 1 and method 2 from one land cover type

| Land cover | Resolution | | |
|---|---|---|---|
| | 250 m (%) | 500 m (%) | 1000 m (%) |
| Shrubs | 5.6 | 6.39 | 7.63 |
| Savanna | 8.6 | 10.09 | 11.9 |

Table 5
Means of difference in LAI (DL) retrievals between method 1 and method 2 from two land cover types

| Land cover | Resolution | | |
|---|---|---|---|
| | 250 m (%) | 500 m (%) | 1000 m (%) |
| Shrubs | 15.1 | 16.8 | 16.3 |
| Savanna | 0.3 | 3.4 | 2.6 |
| Shrubs + Savanna | 4.3 | 4.6 | 5.1 |

One interesting result is that there are some pixels where method 2 overestimates LAI values. This could be possibly noise. Let the overall standard deviation of each coarse resolution pixel's reflectance be (Wang et al., 2001),

$$\sigma = \sqrt{\left(\frac{\sigma_{\mathrm{RED}}}{\overline{\mathrm{RED}}}\right)\left(\frac{\sigma_{\mathrm{NIR}}}{\overline{\mathrm{NIR}}}\right)}. \quad (4)$$

Here, $\overline{\mathrm{RED}}$ ($\overline{\mathrm{NIR}}$) and $\sigma_{\mathrm{RED}}$ ($\sigma_{\mathrm{NIR}}$) are the mean and standard deviation of sub-pixel level reflectance of band 3 (band 4) of coarse resolution pixels, respectively. Pixels that contain homogeneous sub-pixels of reflectance will have a small $\sigma$, and vise versa. Fig. 12 shows $\sigma$ as a function of DL. The $\sigma$ value increases as DL increases. Negative DL values always correspond to the smallest $\sigma$ values. Therefore, the overestimated values are mainly from pixels with the most homogeneous sub-pixel reflectance. It is possible that the overestimated value is either due to limitations of the algorithm or due to measurement errors. When using the savanna LUT, the mean overestimated DL value is $-5.03\%$, $-6.61\%$ and $-2.52\%$, at 250-, 500-, and 1000-m resolutions, respectively. These values are much smaller than the

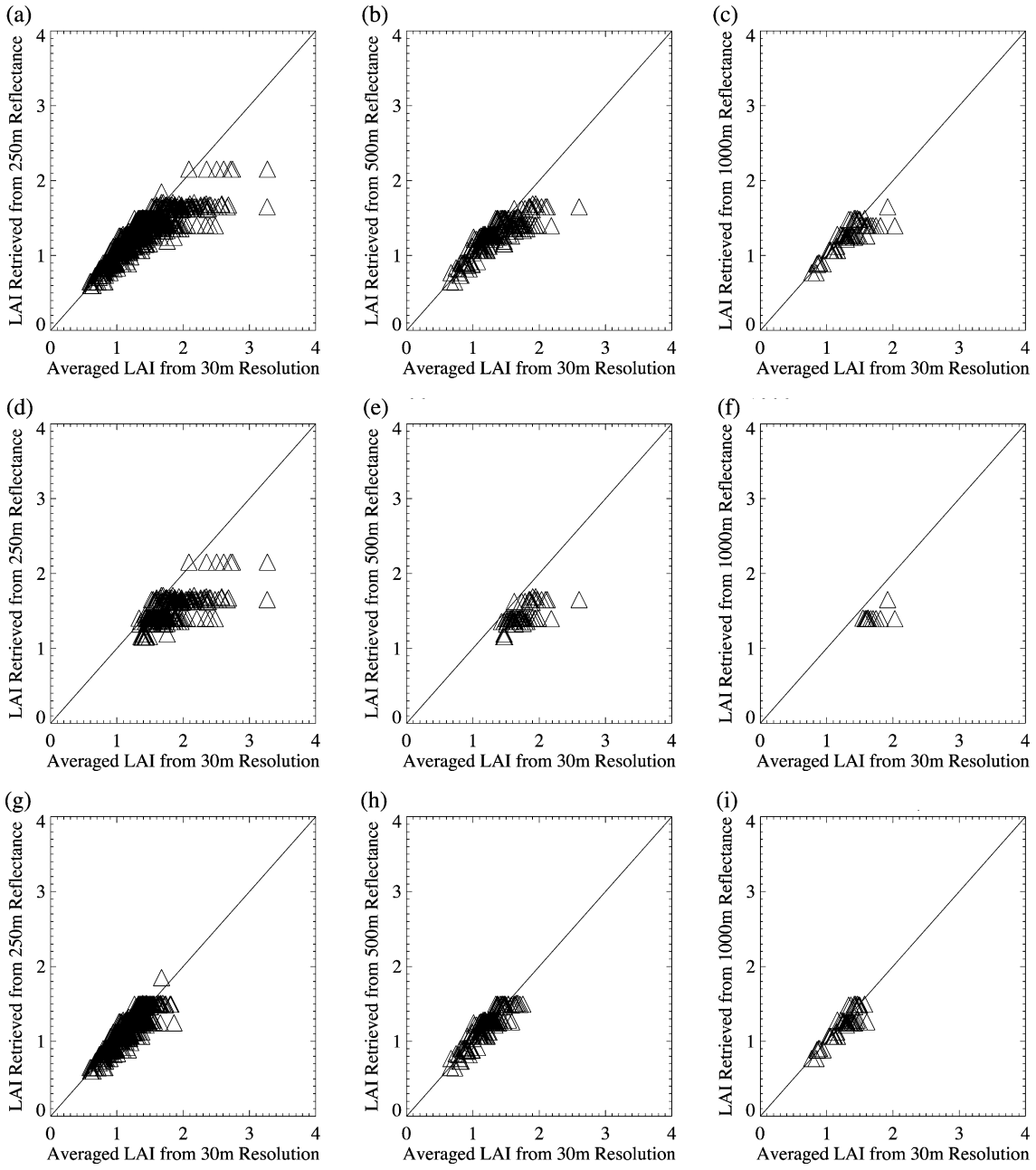


Fig. 13. Pixel-by-pixel comparison of LAI values average from 30-m resolution and retrieved directly from reflectance at resolution of (a) 250 m for all pixels, (b) 500 m for all pixels, (c) 1000 m for all pixels, (d) 250 m for shrub pixels only, (e) 500 m for shrub pixels only, (f) 1000 m for shrub pixels only, (g) 250 m for savanna pixels only, (h) 500 m for savanna pixels only, and (i) 1000 m for savanna pixels only.

mean underestimated DL values (14.34%, 14.14%, and 14.28%, respectively). Therefore, the overestimated value may be considered as noise.

The MODIS LAI algorithm being non-linear will always underestimate the retrieved LAI from coarse resolution reflectance data, even though the overall mean reflectance and NDVI of the image do not change with resolutions. The more heterogeneous the reflectances at fine resolution, the larger the underestimated LAI value will be. As spatial resolution decreases, the underestimation becomes larger. The magnitude of underestimation is dependent on the vegetation type. At 1-km resolution, the algorithm underestimated the LAI values by about 8% from shrub LUT and 12% from savanna LUT at the Maun site (Table 4, Fig. 11), respectively, if the resolution of the data is not considered in the retrieval technique. Therefore, it is necessary to scale the algorithm to resolutions of satellite data (Tian et al., 2000, in press). It should be noted that the MODIS LAI and FPAR operational algorithm addresses this issue explicitly through canopy structure dependent parameters, which imbue scale dependence to the algorithm via modification to the LUTs (Tian et al., 2000; Myneni et al., in press).

### 5.3. Non-linearity and pixel mixture in LAI retrievals from two land cover types

When resolution decreases from 30 to 1000 m, coarse resolution pixels may contain fractions of different land cover types. The coarse resolution LAI values will be influenced by both the non-linearity of the algorithm and cover mixture. We estimated LAI values over the $10 \times 10$ km area from the coarse resolution reflectance by considering the actual land cover type (two types). Table 5 lists the mean DL values for savanna and shrubs, and the overall estimation (shrubs + savanna). Fig. 13 shows a pixel-by-pixel comparison between LAI from method 1 and method 2. Shrubs have higher DL values compared with Table 4, which means that the underestimation becomes larger when both the non-linearity and pixel mixture influence the retrievals. The savanna, on the other hand, show much smaller DL values. This should be interpreted cautiously—LAI from shrubs will always be underestimated, but LAI from savanna could be over- or underestimated depending on the fine scale heterogeneity (see Appendix A). Our results from this analysis indicate that the MODIS algorithm will underestimate LAI values by about 5% in total from the 1-km resolution data over the Maun site if we did not scale the algorithm to the data resolution.

## 6. Concluding remarks

Validation of global data products is crucial, both to establish the accuracy of the products for the science-user community and to provide feedback to improve the data processing algorithms (Cohen & Justice, 1999). Our validation efforts are aimed not only at testing the accuracy of the LAI product, but also to gain an understanding of the causes of errors, and thus provide feedback for potential improvement in second-generation MODIS products. In this two-part series, we attempt to assess the uncertainty of the MODIS LAI product via comparisons with ground and high-resolution satellite data, and provide guidance for field data collection and sampling strategies.

In this paper (Part I), we first tested the LAI retrievals from 30-m resolution ETM+ data with field measurements from the SAFARI 2000 wet season campaign, and then compared the validated LAI fields with those retrieved from MODIS data (250-, 500-, and 1000-m resolutions) simulated from ETM+ data. Because of the high variance of LAI measurements over short distances and mismatch of pixels between the measurements and the image, a patch-by-patch comparison method, which is more realistically implemented on a routine basis for validation, was proposed. Consistency between LAI retrievals from 30 m ETM+ data and field measurements indicates good performance of the algorithm. The estimation for a spatially heterogeneous scene from the MODIS LAI algorithm depends strongly on the spatial resolution of the scene image. As a non-linear model, the MODIS algorithm always underestimates the retrieved LAI from coarse resolution reflectance data. The magnitude of underestimation, dependent on the vegetation type, increases as spatial resolution decreases or heterogeneity increases. LAI over the Maun site will be underestimated by about 5% from 1-km MODIS data if resolution of the data is not considered in the retrieval technique. Based on the patch-by-patch comparison detailed here, Part II provides sampling strategies for validation of coarse resolution satellite products through hierarchical decomposition of ETM+ data from Maun, Harvard Forest and Ruokulahti Forest.

## Acknowledgements

We thank the three anonymous reviewers for their professional and insightful comments. We also thank individuals who participated in the SAFARI 2000 wet season, Harvard Forest, and Ruokolahti Forest campaigns, especially Luanne Otter, Robert Scholes, Seth Hoffman, and Pauline Stenberg; the people who were essential in acquiring and processing the ETM+ and IKONOS data, especially Jeff Morisette, Heikki Smolander; and all the various other field participants who made various measurements that we used, especially Grace Smith, and Karyn Tabor. This study was part of the SAFARI 2000 Southern African Regional Science Initiative. The research was supported by NASA through MODIS Contract NAS5-96061.

## Appendix A. Effect of non-linearity and pixel mixture on LAI retrievals

Coarse resolution LAI can be derived by two different methods: LAI derived from arithmetic averaging of LAI values retrieved from fine resolution data (method 1) and LAI retrieved from coarse resolution sensor data directly (method 2). It is clear that the LAI value from method 1 is the correct value. In this appendix, we discuss situations under which the LAI values from method 2 will be under- or overestimated.

The MODIS LAI algorithm is a non-linear and biome type dependent model. Let us assume that $f$ represents the relation between LAI and surface reflectances derived from fine resolution data, i.e., $LAI_{i,j}=f_i$ (reflectance). Here, i represents the land cover type (1 to 6), j represents sub-pixel number. For a coarse resolution pixel, it could be a pure pixel, or a mixed pixel that consists of sub-pixels with other land cover types. For simplicity, let us assume that there are only two sub-pixels, with reflectance of $r_1$ and $r_2$, respectively, in a coarse resolution pixel. Obviously, the two sub-pixels are either the same land cover type or two different cover types. We discuss this below separately.

### A.1. One land cover type

If the two sub-pixels are from the same land cover type, for example, savanna, we have

$$\mathrm{LAI}_{1,1}=f_1(r_1), \tag{A.1}$$

$$\mathrm{LAI}_{1,2}=f_1(r_2). \tag{A.2}$$

The mean LAI of the coarse resolution pixel in method 1 is

$$\mathrm{LAI}_{\text{method 1}}=\frac{\mathrm{LAI}_{1,1}+\mathrm{LAI}_{1,2}}{2}=\frac{f_1(r_1)+f_1(r_2)}{2}. \tag{A.3}$$

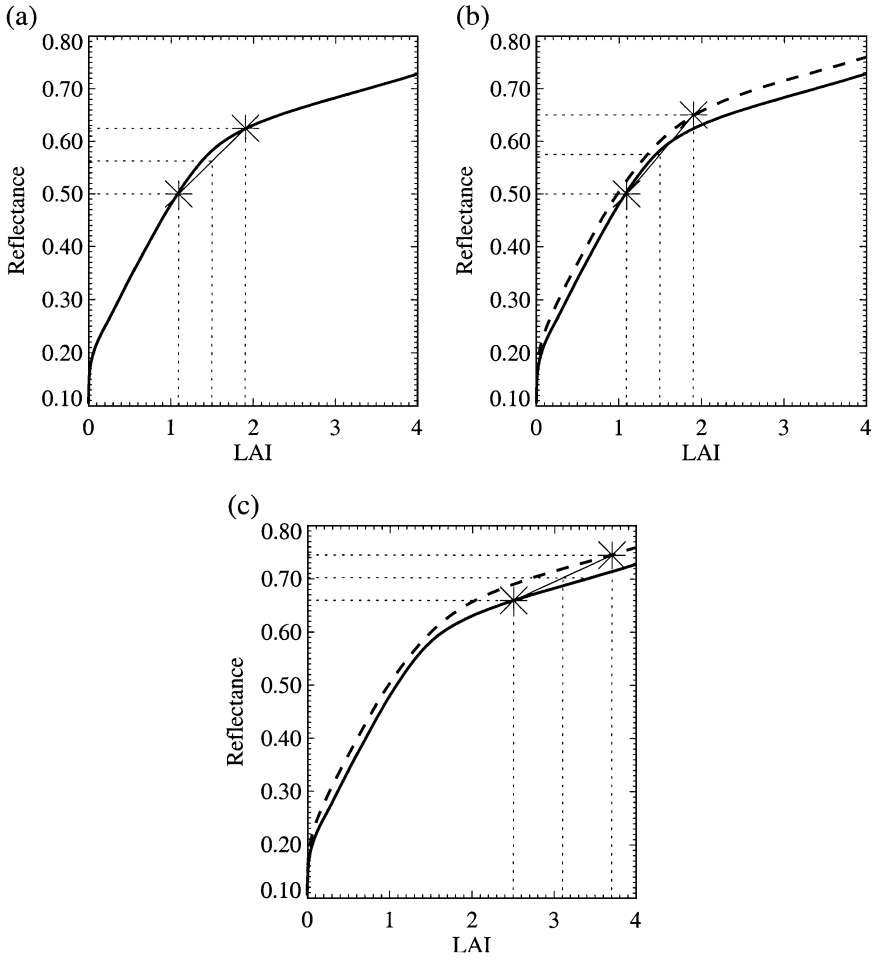


Fig. 14. Relation between LAI and surface reflectance at 30-m resolution for (a) savanna (solid line), (b) savanna (solid line) and shrubs (dash line), which shows that the retrieved LAI from coarse resolution reflectance data is underestimated for both savanna and shrubs, and (c) savanna (solid line) and shrubs (dash line), which shows that the retrieved LAI from the coarse resolution reflectance data is underestimated for shrubs and overestimated for savanna. See Appendix A for further clarification.

In method 2, the reflectance of the coarse resolution pixel is $r=(r_1+r_2)/2$. If the function $f$ is used to retrieve the LAI value, then

$$\mathrm{LAI}_{\mathrm{method\ 2}} = f_1(r) = f_1\left(\frac{r_1+r_2}{2}\right). \quad (A.4)$$

Fig. 14a shows the relation between LAI and reflectance at 30-m resolution for savanna (solid line). It is clear that $\mathrm{LAI}_{\mathrm{method\ 1}}$ is larger than $\mathrm{LAI}_{\mathrm{method\ 2}}$. Therefore, the retrieved LAI directly from coarse resolution reflectance data underestimates the LAI value.

### A.2. Two different land cover types

If the two sub-pixels are of two different land cover types, class 1 and class 2, two different functions $f_1$ and $f_2$ are needed to represent the relation between LAI and reflectance at the fine resolution. Thus,

$$\mathrm{LAI}_{1,1} = f_1(r_1), \quad (A.5)$$

$$\mathrm{LAI}_{2,2} = f_2(r_2). \quad (A.6)$$

The mean LAI for the coarse resolution pixel in method 1 is

$$\mathrm{LAI}_{\mathrm{method\ 1}} = \frac{\mathrm{LAI}_{1,1}+\mathrm{LAI}_{2,2}}{2} = \frac{f_1(r_1)+f_2(r_2)}{2}. \quad (A.7)$$

In method 2, the retrieved LAI value of the coarse resolution pixel is dependent on which function, $f_1$ and $f_2$, is used. It is either

$$\mathrm{LAI}_{\mathrm{method\ 2,\ class\ 1}} = f_1(r) = f_1\left(\frac{r_1+r_2}{2}\right), \quad (A.8)$$

if pixel is defined as class 1, or

$$\mathrm{LAI}_{\mathrm{method\ 2,\ class\ 2}} = f_2(r) = f_2\left(\frac{r_1+r_2}{2}\right), \quad (A.9)$$

is defined as class 2.

Fig. 14b and c shows the relation between LAI and reflectance for class 1 (savanna, solid line), and for class 2 (shrubs, dash line), at 30-m resolution. Whether the retrieved LAI directly from the coarse resolution reflectance data is under- or overestimated depends on the location of reflectance of class 1 and class 2 in the reflectance-LAI space at the fine resolution. There are two possible cases.

#### A.2.1. Case A

If the location of the reflectance of class 1 and class 2 is distributed as shown in Fig. 14b, then

$$\mathrm{LAI}_{\mathrm{method\ 1}} > \mathrm{LAI}_{\mathrm{method\ 2,\ class\ 1}} > \mathrm{LAI}_{\mathrm{method\ 2,\ class\ 2}}. \quad (A.10)$$

This means that the retrieved LAI for the coarse resolution reflectance data is underestimated irrespective of the biome classification.

#### A.2.2. Case B

If the location of the reflectance of class 1 and class 2 is distributed as shown in Fig. 14c, then

$$\mathrm{LAI}_{\mathrm{method\ 2,\ class\ 1}} > \mathrm{LAI}_{\mathrm{method\ 1}} > \mathrm{LAI}_{\mathrm{method\ 2,\ class\ 2}}. \quad (A.11)$$

This means that the retrieved LAI directly from the coarse resolution reflectance data is underestimated if it is defined as class 2 or overestimated if it is defined as class 1.

These results indicate that class 2 (shrubs) is always underestimated while class 1 (savanna) could be under- or overestimated.

## References


Barker, J. L., Markham, B. L., & Burelbach, J. (1992). *MODIS image simulation from Landsat TM imagery.* ASPRS/ACSM/RT 92 technical paper, *1*, 156–165.

Beaulieu, J.-M., & Goldberg, M. (1989). Hierarchy in picture segmentation: a stepwise optimization approach. *IEEE Transactions on Pattern Analysis and Intelligence*, *11*, 150–163.

Bonan, G. B. (1995). Land–atmosphere interactions for climate system models: coupling biophysical, biogeochemical, and ecosystem dynamical processes. *Remote Sensing of Environment*, *51*, 57–73.

Buermann, W., Dong, J., Zeng, X., Myneni, R. B., & Dickinson, R. E. (2001). Evaluation of the utility of satellite-based vegetation leaf area index data for climate simulations. *Journal of Climate*, *14*(17), 3536–3550.

Chen, J. M. (1999). Spatial scaling of a remotely sensed surface parameter by contexture. *Remote Sensing of Environment*, *69*, 30–42.

Cohen, W. B., & Justice, C. O. (1999). Validating MODIS terrestrial ecology products: linking in situ and satellite measurements. *Remote Sensing of Environment*, *70*, 1–3.

Cushnie, J. L. (1987). The interactive effect of spatial resolution and degree of internal variability within land-cover types on classification accuracies. *International Journal of Remote Sensing*, *8*(1), 15–29.

Dowty, P., Frost, P., Lesolle, P., Midgley, G., Otter, L., Privette, J., Ramontsho, J., Ringrose, S., Scholes, B., & Wang, Y. (2000). Summary of the SAFARI 2000 wet season field campaign along the Kalahari transect. *The Earth Observer*, *12*, 29–34.

Hall, F. G., Huemmrich, K. F., Goetz, S. J., Sellers, P. J., & Nickeson, J. E. (1992). Satellite remote sensing of surface energy balance: success, failures, and unresolved issues in FIFE. *Journal of Geophysical Research*, *97*(D17), 19061–19089.

Häme, T., Stenberg, P., Andersson, K., Rauste, Y., Kennedy, P., Folving, S., & Sarkeala, J. (2001). AVHRR-based forest proportion map of the Pan-European area. *Remote Sensing of Environment*, *77*, 76–91.

Hautecoeur, O., & Leroy, M. (2000). An accuracy assessment experiment of the BRDF measured at coarse spatial resolution from space. *International Journal of Remote Sensing*, *21*(15), 2957–2963.

Justice, C., Belward, A., Morisette, J., Lewis, P., Privette, J., & Baret, F. (2000). Developments in the 'validation' of satellite sensor products for the study of the land surface. *International Journal of Remote Sensing*, *21*(17), 3383–3390.

Knyazikhin, Y., Glassy, J., Privette, J. L., Tian, Y., Lotsch, A., Zhang, Y., Wang, Y., Morisette, J. T., Votava, P., Myneni, R. B., Nemani, R. R., &

Running, S. W. (1999). *MODIS Leaf Area Index (LAI) and Fraction of Photosynthetically Active Radiation Absorbed by Vegetation (FPAR) Product (MOD15) Algorithm*, Theoretical Basis Document, NASA Goddard Space Flight Center, Greenbelt, MD 20771, USA.

Knyazikhin, Y., Martonchik, J. V., Diner, D. J., Myneni, R. B., Verstraete, M. M., Pinty, B., & Gobron, N. (1998). Estimation of vegetation canopy leaf area index and fraction of absorbed photosynthetically active radiation from atmosphere-corrected MISR data. *Journal of Geophysical Research*, *103*, 32239–32256.

Knyazikhin, Y., Martonchik, J. V., Myneni, R. B., Diner, D. J., & Running, S. W. (1998). Synergistic algorithm for estimating vegetation canopy leaf area index and fraction of absorbed photosynthetically active radiation from MODIS and MISR data. *Journal of Geophysical Research*, *103*, 32257–32275.

Lewis, P., Disney, M. I., Barnsley, M. J., & Muller, J.-P. (1999). Deriving albedo maps for HAPEX-Sahel from ASAS data using kernel-driven BRDF models. *Hydrology and Earth System Sciences*, *3*, 1–13.

Li-COR INC. (1992). *LAI-2000 plant canopy analyzer instruction manual*. (pp. 4–12).

Lucht, W., Hyman, A. H., Strahler, A. H., Barnsley, M. J., Hobson, P., & Muller, J.-P. (2000). A comparison of satellite-derived spectral albedos to ground-based broadband albedo measurements modelled to satellite spatial scale for a semidesert landscape. *Remote Sensing of Environment*, *74*, 85–98.

MacDonald, R. B., & Hall, F. G. (1980). Global crop forecasting. *Science*, *208*, 670–679.

Markham, B. L., & Townshend, J. R. G. (1981). Landcover classification accuracy as a function of sensor spatial resolution. *Proceedings of the 15th international symposium on Remote Sensing of Environment held in Ann Arbor, Michigan, U.S.A.* (pp. 1075–1090).

Myneni, R. B., Knyazikhin, Y., Privette, J. L., Glassy, J., Tian, Y., Wang, Y., Hoffman, S., Song, X., Zhang, Y., Smith, G. R., Lotsch, A., Friedl, M., Morisette, J. T., Votava, P., Nemani, R. R., & Running, S. W. (2002). Global products of vegetation leaf area and fraction of absorbed PAR from year one of MODIS data. *Remote Sensing of Environment* (in press).

Pax-Lenney, M., & Woodcock, C. E. (1997). The effect of spatial resolution on the ability of monitor the status of agricultural lands. *Remote Sensing of Environment*, *61*, 210–220.

Privette, J. L., Asner, G. P., Conel, J., Huemmrich, K. F., Olson, R., Rango, A., Rahman, A. F., Thome, K., & Walter-Shea, E. A. (2000). The EOS prototype validation exercise (PROVE) at Jornada: overview and lessons learned. *Remote Sensing of Environment*, *74*, 1–12.

Privette, J. L., Myneni, R. B., Knyazikhin, Y., Mukufute, M., Roberts, G., Tian, Y., Wang, Y., & Leblanc, S. G. (2002). Early spatial and temporal validation of MODIS LAI product in Africa. *Remote Sensing of Environment* (in press).

Rahman, H., & Didieu, G. (1994). SMAC: a simplified method for the atmospheric correction of satellite measurements in the solar spectrum. *International Journal of Remote Sensing*, *15*, 123–143.

Running, S. W. (1990). A bottom-up evolution of terrestrial ecosystem modeling theory, and ideas toward global vegetation modeling. In D. Ojima (Ed.), *Modeling the earth system* (pp. 263–280). Boulder, CO: UCAR/Office for Interdisciplinary Earth Studies.

Running, S. W., Nemani, R. R., Peterson, D. L., Band, L. E., Potts, D. F., Pierce, L. L., & Spanner, M. A. (1989). Mapping regional forest evapotranspiration and photosynthesis by coupling satellite data with ecosystem simulation. *Ecology*, *70*, 1090–1101.

Scholes, R. J., Dowty, P. R., Caylor, K., Parsons, D. A. B., Frost, P. G. H., & Shugart, H. H. (2002). Trends in savanna structure and composition on an aridity gradient in the Kalahari. *Journal of Vegetation Science (*in press).

Stroeve, J. C., Box, J. E., Fowler, C., Haran, T., & Key, J. (2001). Intercomparison between *in situ* and AVHRR polar pathfinder-derived surface albedo over Greenland. *Remote Sensing of Environment*, *75*, 360–374.

Swap, R. J., & Annegarn, H. J. (1999). Southern African regional science initiative: Safari 2000 science plan. http://safari.gecp.virginia.edu.

Tian, Y., Wang, Y., Zhang, Y., Knyazikhin, Y., Bogaert, J., & Myneni, R. B. (2002). Radiative transfer based scaling of LAI retrievals from reflectance data of different resolutions. *Remote Sensing of Environment* (in press).

Tian, Y., Zhang, Y., Knyazikhin, Y., Myneni, R. B., Glassy, J. M., Dedieu, D., & Running, S. W. (2000). Prototyping of MODIS LAI and FPAR algorithm with LASUR and LANDSAT data. *IEEE Transactions on Geoscience and Remote Sensing*, *38*(5), 2387–2401.

Turner, D. P., Cohen, W. B., Kennedy, R. E., Fassnacht, K. S., & Briggs, J. M. (1999). Relationships between leaf area index, fapar, and net primary production of terrestrial ecosystems. *Remote Sensing of Environment*, *70*, 52–68.

Wang, Y., Tian, Y., Zhang, Y., El-Saleous, N., Knyazikhin, Y., Vermote, E., & Myneni, R. B. (2001). Investigation of product accuracy as a function of input and model uncertainties: case study with SeaWiFS and MODIS LAI/FPAR algorithm. *Remote Sensing of Environment*, *78*, 296–311.

Weiss, M., Beaufor, L., Baret, F., Allard, D., Bruguier, N., & Marloie, O. (2001). Leaf area index measurements at different scales for the validation of large swath satellite sensors: first results of the VALERI project. *Proceeding of the 8th international symposium on physical measurements and signatures in remote sensing* (pp. 125–130).

Woodcock, C. E., Collins, J. B., & Jupp, D. L. B. (1997). Scaling remote sensing models. In P. R. Van Gardingen, G. M. Foody, & P. J. Curran (Eds.), *Scaling-up from cell to landscape* (pp. 61–77). United Kingdom: Cambridge.

Woodcock, C. E., & Harward, V. J. (1992). Nested-hierarchical scene models and image segmentation. *International Journal of Remote Sensing*, *13*(16), 3167–3187.

Woodcock, C. E., & Strahler, A. H. (1987). The factor of scale in remote sensing. *Remote Sensing of Environment*, *21*, 311–332.